BACCHUS

Impact of Biogenic versus Anthropogenic emissions on Clouds and Climate: towards a Holistic UnderStanding

Collaborative Project

SEVENTH FRAMEWORK PROGRAMME
ENV.2013.6.1-2

Atmospheric processes, eco-systems and climate change

Grant agreement no: 603445

Deliverable number:	**D4.5**
Deliverable name:	Future scenario simulations with three ESMs, including an assessment of the role of future ship emissions with an ice-free Arctic Ocean.
WP number:	4
Delivery date:	Project month 54 (31/05/2018)
Actual date of submission:	24/05/2018
Dissemination level:	PU
Lead beneficiary:	ETHZ
Responsible scientist/administrator:	Ulrike Lohmann (ETHZ)
Estimated effort (PM):	52
Contributor(s):	Katty Huang (ETHZ), David Neubauer (ETHZ), Anina Gilgen (ETHZ), Risto Makkonen (UHEL), Stijn Hantson (KIT) Almuth Arneth (KIT)
Estimated effort contributor(s) (PM):	ETHZ:18 (+9 unpaid) PM , UHEL: 12 PM, KIT: 12 (+1 unpaid) PM
Internal reviewer:	Risto Makkonen (UHEL)

Summary of results

1. Setup, tuning and evaluation of Earth System Models (ESMs)

1.1 Setup and model tuning of MPI-ESM1.2-HAM

MPI-ESM1.2-HAM has been set-up and tuned for WP4. It includes the latest version of the global climate model ECHAM6.3 (Stevens et al., 2013) and the latest version of the aerosol module HAM2.3 (Tegen et al., 2018; see Figure 1 for the components of MPI-ESM and MPI-ESM1.2-HAM). Due to the high computational demand (MPI-ESM-HAM is about 4 times slower than MPI-ESM at the same resolution) that is a result of the online computation of aerosol microphysical processes and aerosol-cloud interactions, MPI-ESM1.2-HAM has been set-up for the low resolution of MPI-ESM i.e. T63 horizontal spectral resolution (1.875° x 1.875°), 47 vertical levels (0.01 hPa top level) and a bipolar ocean grid with 1.5° resolution and 40 vertical levels.

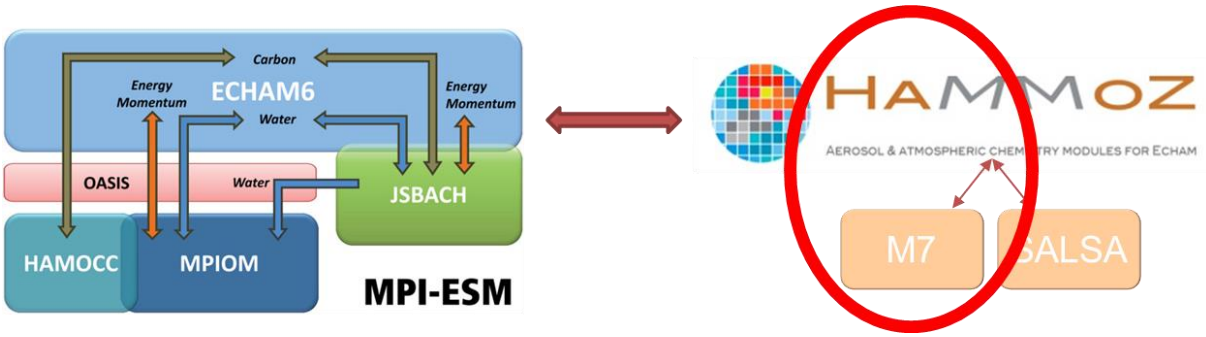

Figure 1: The components of MPI-ESM1.2-HAM are presented. MPI-ESM consists of the atmosphere model ECHAM which includes the land model JSBACH and is coupled via the coupler OASIS to the ocean model MPIOM and the biogeochemistry model HAMOCC. From the aerosol and chemistry package HAMMOZ the aerosol module HAM in the configuration with the M7 modal aerosol size distribution is coupled to MPI-ESM.

For model tuning (calibration of uncertain model parameters) a new tuning strategy (Folini et al., 2018) was applied which allows to use the (computationally expensive) ocean spin-up of MPI-ESM and therefore to save CPU time for spinning up MPI-ESM-HAM. MPI-ESM-HAM is therefore tuned to have the same global mean surface temperature and the same global mean net surface energy flux as MPI-ESM in equilibrium conditions. This tuning strategy allows the simulated ocean in MPI-ESM-HAM to be equilibrated within hundreds of years instead of thousands of years which it would take otherwise for the deep ocean to be in equilibrium. The disadvantage of the strategy is that a similar setup of MPI-ESM must be available (similar model components, resolution and forcing data). The tuning of MPI-ESM1.2-HAM for WP4 was done using Coupled Model Intercomparison Project Phase 5 (CMIP5) forcing data.

1.2 Model evaluation of MPI-ESM and MPI-ESM-HAM

MPI-ESM1.2-HAM was evaluated for pre-industrial and historical simulations and future projections (using the Representative Concentration Pathways (RCP) scenario RCP8.5). For the evaluation, MPI-ESM1.2-HAM was compared to MPI-ESM-LR (low resolution version of MPI-ESM which took part in CMIP5), other CMIP5 models and when possible to observations and re-analysis data. Exemplary parts of this evaluation are presented here. Of particular interest is how an ESM simulates the change in surface temperature from pre-industrial times to

present-day. Figure 2 shows the evolution of the global mean surface temperature during the historical time period. MPI-ESM1.2-HAM simulates temperature decreases after major volcanic eruptions of a similar magnitude as was observed. While the surface temperature evolutions during the historical time period of MPI-ESM-LR and MPI-ESM1.2-HAM lie within the range of the CMIP5 models, MPI-ESM-LR is warming more than observed (0.2 K warmer in 1961-1990 than observed) and MPI-ESM1.2-HAM is warming less than observed (0.1 K colder in 1961-1990 than observed). The differences in historical warming between MPI-ESM-LR and MPI-ESM1.2-HAM could be due to a different climate sensitivity of the models (MPI-ESM-LR uses a one-moment cloud microphysics scheme and MPI-ESM1.2-HAM uses a two-moment cloud microphysics scheme and both models differ in their tuning) or due to differences in the aerosol forcing (MPI-ESM-LR uses a climatology for aerosol optical properties to compute the aerosol radiative forcing whereas MPI-ESM1.2-HAM computes the aerosol radiative forcing as well as its adjustments, i.e. the effective radiative forcing online). Rotstayn et al. (2015) found that for the historical time period the aerosol forcing, not the greenhouse gas warming, controls the spread in global mean surface temperature change in CMIP5 models.

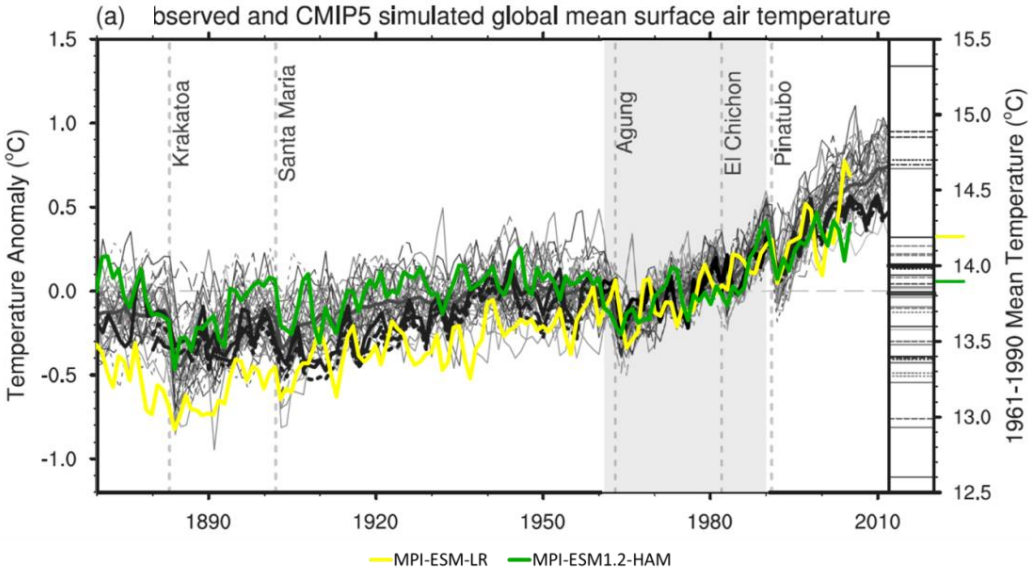

Figure 2: Historical global mean surface temperature anomaly evolution. The anomalies are differences from the 1961-1990 mean temperature (the time period 1961-1990 is shaded grey). Thin grey lines refer to individual CMIP5 models, the thick grey line to the CMIP5 multi-model mean, the thick black lines to different observations, the yellow line to MPI-ESM-LR and the green line to MPI-ESM1.2-HAM. The vertical dashed lines show the times of major volcanic eruptions. On the right side the global mean surface temperature for the time period 1961-1990 is shown (coloring is the same as on the left). Adapted from Flato et al. (2013).

They found a strong correlation between global mean surface temperature change and aerosol radiative forcing which is shown in Figure 3a. CMIP5 models with a strong (more negative) aerosol forcing have a weaker increase in global mean surface temperature and models with a weaker (less negative) aerosol forcing have a stronger increase in global mean surface temperature. MPI-ESM1.2-HAM also falls onto the regression line of Rotstayn et al. (2015). The global mean surface temperature change is weaker in MPI-ESM1.2-HAM than observed and the aerosol forcing is stronger than what can be inferred from the observed global mean surface temperature change. On the contrary, the global mean surface temperature change is stronger in MPI-ESM-LR than observed and the aerosol forcing is

weaker than the inferred aerosol forcing. Therefore, the different historical warmings between MPI-ESM-LR and MPI-ESM1.2-HAM can be explained by the differences in aerosol radiative forcing between the models. Figure 3b shows next to the historical temperature trend also the temperature increase in the 21st century for the RCP8.5 scenario for CMIP5 models, MPI-ESM-LR and MPI-ESM1.2-HAM. The warming of MPI-ESM-LR and MPI-ESM1.2-HAM in the RCP8.5 scenario is very close to the CMIP5 multi-model mean. Although aerosol emissions decrease in the 21st century in the RCP8.5 scenario (and therefore differences in aerosol radiative forcing presumably become less important) and greenhouse gas emission increase, it is still remarkable that MPI-ESM-LR and MPI-ESM1.2-HAM show such a similar surface temperature increase and therefore climate sensitivity. As mentioned above, due to the different cloud schemes and the differences in tuning a different climate sensitivity could be expected. The coincidence of both models having a similar climate sensitivity allows for an easier interpretation of differences between the two models in future projections (at least in the RCP8.5 scenario).

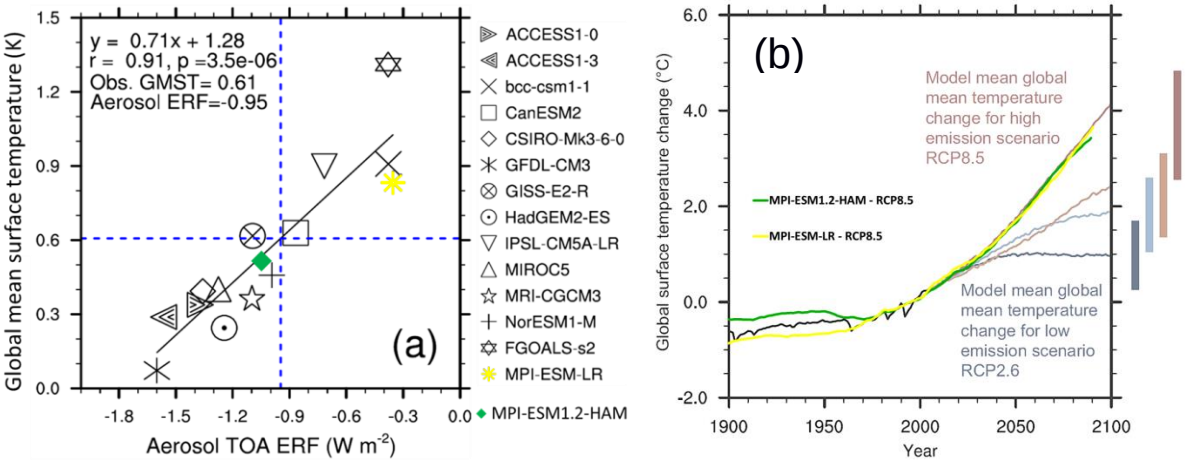

Figure 3: a) Correlation between top of the atmosphere (TOA) aerosol effective radiative forcing (ERF: 2000 minus 1850) and global mean surface temperature change (1860-2000) for CMIP5 models, MPI-ESM-LR and MPI-ESM1.2-HAM. The dashed horizontal line shows the observed increase in global mean surface temperature and the dashed vertical line is inferred from the regression line. Adapted from Rotstayn et al. (2015); b) Surface temperature anomaly evolution for different RCP scenarios of CMIP5 models (historical-black, RCP2.6-dark blue, RCP4.5-light blue, RCP6.0-orange, RCP8.5-blue) and for MPI-ESM-LR and MPI-ESM1.2-HAM RCP8.5. The vertical bars on the right-hand side show likely warming by the end of the 21st century. The anomalies are differences from the 1986-2005 mean temperature. Adapted from Collins et al. (2013).

Next to the evaluation of the surface temperature we present here an evaluation of the ocean circulation and of sea ice in the Northern Hemisphere. Figure 4 shows the annual mean of the Atlantic meridional overturning circulation (AMOC) for the time period 1900-2005 for MPI-ESM-LR and MPI-ESM1.2-HAM. The AMOC consists of a clockwise rotating North Atlantic Deep Water (NADW) cell and the counterclockwise rotating Antarctic Bottom Water (AABW) cell. The NADW cell in MPI-ESM1.2-HAM is stronger than in MPI-ESM-LR. The observed strength of the NADW cell at 26.5° N has its maximum (18.7 Sv) at a depth of 1000 m (Jungclaus et al., 2013 and references therein), similar to the depth where both models simulate the maximum. The boundary between the NADW and AABW cells is at 3000 m in the models while it was observed to be between 3500 and 4000 m. Although both models show differences to the

observations, the differences between MPI-ESM-LR and MPI-ESM1.2-HAM are smaller than between other CMIP5 models (not shown).

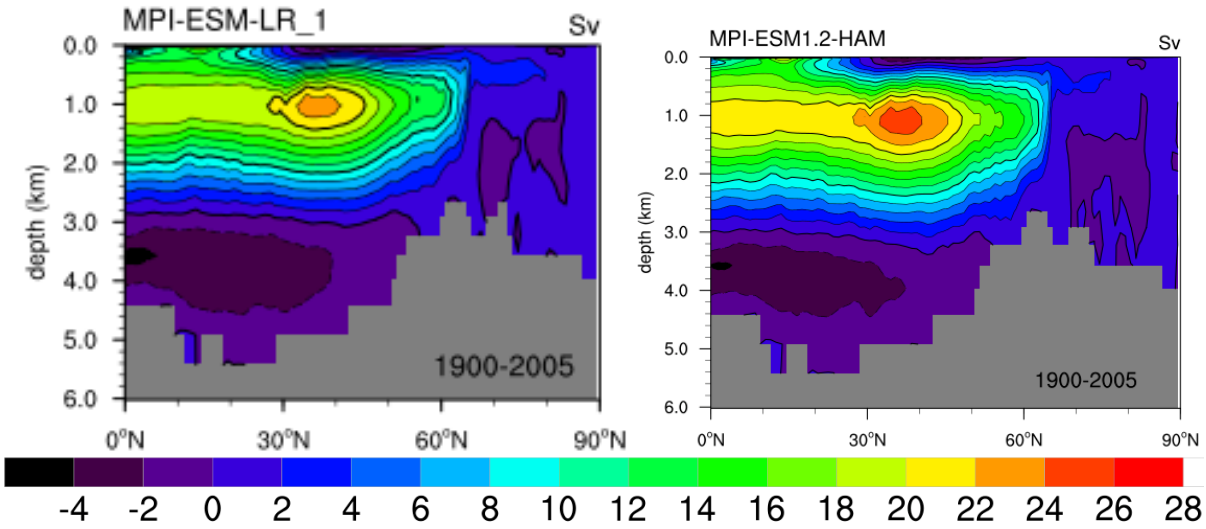

Figure 4: The annual mean of the Atlantic meridional overturning circulation for the time period 1900-2005 of MPI-ESM-LR and MPI-ESM1.2-HAM is shown. The figure was created using the Climate Variability Diagnostics Package (CVDP; Philips et al., 2014).

Figure 5 shows the change in sea ice extent in the Northern Hemisphere. In Figure 5a, the sea ice extent change during the time of the maximum sea ice extent (February) is shown. The decrease in sea ice in MPI-ESM-LR and MPI-ESM1.2-HAM during the historical time period agrees well with observations but in the future (RCP8.5 scenario) it is weaker than in the CMIP5 multi-model mean (at the upper range of the CMIP5 models for the RCP8.5 scenario). Similar to the global mean surface temperature change, the decrease in the RCP8.5 scenario in the Northern Hemisphere sea ice at its maximum extent is similar in both models. The projection of the minimum sea ice extent in September on the contrary differs strongly between the two models (Figure 5b). While MPI-ESM-LR shows a weaker decrease throughout the 21st century than the CMIP5 multi-model mean (at the upper end of the range of the CMIP5 models for the RCP8.5 scenario), MPI-ESM1.2-HAM simulates a stronger decrease in sea ice than the CMIP5 multi-model mean (at the lower end of the range of the CMIP5 models for the RCP8.5 scenario). This stronger decrease in September agrees better with the observed trend.

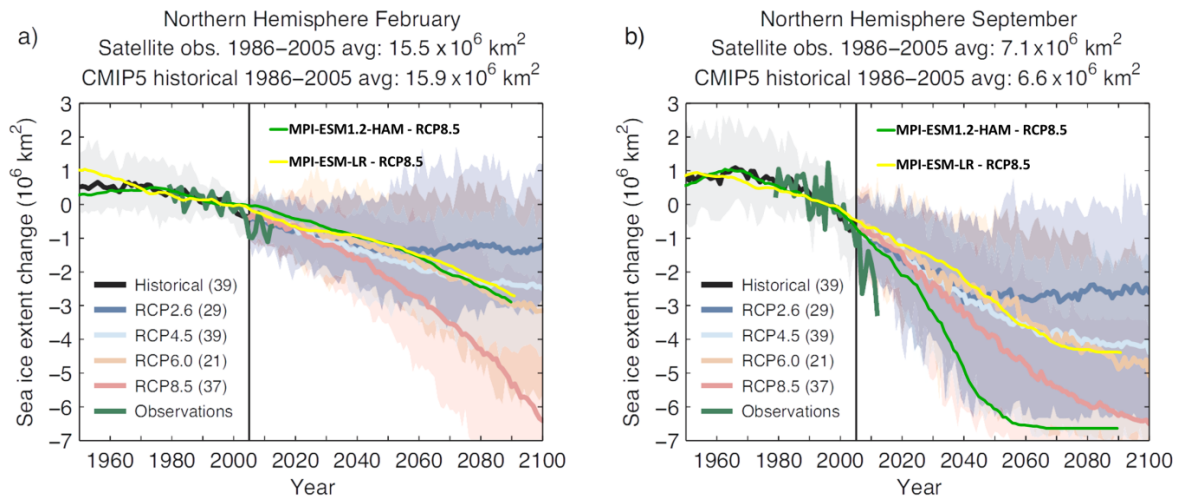

Figure 5: Sea ice extent anomaly evolution for different RCP scenarios of CMIP5 models (historical-black, RCP2.6-dark blue, RCP4.5-light blue, RCP6.0-orange, RCP8.5-blue), observations (dark green) and for MPI-ESM-LR and MPI-ESM1.2-HAM RCP8.5 for a) Northern Hemisphere February (maximum sea ice extent) and b) Northern Hemisphere September (minimum sea ice extent). Shading indicates the 5% to 95% range of the CMIP5 model ensemble. Sea ice extent is the sum of the area of the grid boxes where the sea ice concentration exceeds 15%. The anomalies are differences from the 1986-2005 sea ice extent. Adapted from Collins et al. (2013).

Massonnet et al. (2012) found a correlation between the projected September Arctic sea ice change in CMIP5 models and the simulation of present day Arctic sea ice. The September Arctic sea ice extent, the annual mean sea ice volume, the past trend in September Arctic sea ice extent and the mean seasonal cycle of sea ice extent correlate with the future decline in Arctic sea ice. Based on these empirical relationships several CMIP5 models were selected by Massonnet et al. (2012) which simulate the present-day Arctic sea ice well (Figure 6). MPI-ESM1.2-HAM (added in Figure 6) has also a good representation of present day Arctic sea ice except for the mean seasonal cycle of sea ice extent, which is underestimated (not shown). The Arctic sea ice decrease in the 21st century of MPI-ESM1.2-HAM agrees well the CMIP5 models selected by Massonnet et al. (2012). All these models show an ice-free Arctic in September in the 2nd half of the 21st century in the RCP8.5 scenario.¨

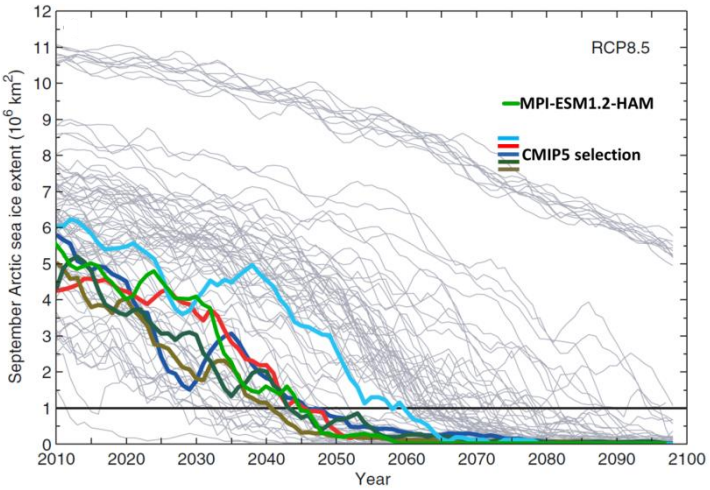

Figure 6: Sea ice extent evolution for the RCP8.5 scenario of CMIP5 models (including all ensemble members; thin grey lines), selected CMIP5 models (following Massonnet et al., 2012) and MPI-ESM1.2-HAM. Adapted from Collins et al. (2013).

2. Investigating changes in heterogeneous ice nucleation in the Arctic in the future

Using the newly tuned MPI-ESM1.2-HAM model, a 55-year simulation was performed starting from year 2000 following a historical simulation. The business-as-usual RCP8.5 scenario is used for prescribing future anthropogenic emissions. To investigate changes, the present-day (PD; averaged between 2005 and 2014) period is contrasted against the future (averaged between 2045 and 2054).

The Arctic was chosen for the region of analysis as this is the part of the world where the most drastic environmental changes are expected in the next decades. Focus is placed on heterogeneous ice nucleation as the Arctic environment is favourable for persistent mixed-phase clouds (Shupe 2011, Morrison et al., 2012), in which heterogeneous ice nucleation plays an important role (Pruppacher and Klett, 1997).

2.0.1 Representation of heterogeneous ice nucleation in the model

Heterogeneous ice nucleation refers to the ice formation process involving an ice nucleating particle (INP) which decreases the energy barrier needed for initiation of an ice embryo (Kanji et al., 2017). In the current study, such processes are only considered in the mixed-phase temperature range (0 to -35 °C), as at colder temperatures, ice is assumed to form homogeneously (without the help of INPs). While there is still much research being conducted on identifying and describing INPs (Kanji et al., 2017), we consider two species in our model which can nucleate ice: dust and marine organic aerosol (MOA). Both are assumed to only act in the immersion freezing mode, where the INP needs to be immersed in a droplet before initiating ice formation. The number of immersed particles is dependent on the number of particles activated into cloud droplets following Köhler theory and the relative mass fraction of the INP species compared to the total mass of the activated aerosol. A more thorough description of the representation of the freezing of especially MOA in our model is described in Huang et al. (2017).

2.1 Changes in aerosol concentrations

One of the key drivers for potential changes in heterogeneous ice nucleation is the change in aerosol properties in the future. Following the RCP scenario, anthropogenic aerosol emissions are generally expected to decrease in the future following technological and economic developments. This would lead to lower sulphate, black carbon (BC), and organic carbon (OC) emissions in the lower latitudes (especially North Hemisphere mid-latitudes) in the future that translates to fewer transported aerosol particles reaching the Arctic. The more dominating effect in our model, however, is the decrease in dust burden in the future, driven mainly by the decrease in dust emissions from northern Africa. The cause for such change can be traced back to the greening of the Sahel region in our model. While the source region for dust emission is fixed in our model regardless of changes in the land cover, greening of the previously more barren land leads to increased surface roughness and thus lower near-ground wind speeds. Parametrised dust emissions following Tegen et al. (2002) and Cheng et al. (2008) are highly dependent on the 10-metre wind speed. Greening of the Sahel region therefore leads to significant decreases in dust emissions from the area. As the Sahara is one of the most important sources of dust on the globe, this results in significant decreases in dust burden,

especially in the Northern Hemisphere, and subsequently much lower aerosol transport into the Arctic. Similar greening in the next decades is also observed by Bathiany et al. (2014) in three CMIP5 models, and the reasoning is attributed to fertilization of vegetation by the increased CO_2 levels. They noted, however, that due to mainly differing balancing responses of precipitation and CO_2 fertilization, the greening effect does not persist after 2050 across models, and the robustness of future greening or browning trends in the Sahel is still uncertain.

Locally in the Arctic, on the other hand, sea spray emissions of sea salt and MOA increase in the future due to sea ice melt and subsequent exposure of the Arctic Ocean. In particular, this leads to a statistically significant increase in sea salt mass concentration of 60 to 100 % below 2 km altitude (relative to the mean concentration in present day (PD) and future). The change is less significant at higher altitudes as long-range transport becomes more relevant. MOA concentrations also show a similar increasing trend near the surface in the future, though with a rather more abrupt change to a decreasing trend aloft. Since the overall concentration of MOA is relatively low, however, the changes are generally not statistically significant.

The overall aerosol size, which can influence the number of aerosol particles activated into cloud droplets and therefore the number of immersed INPs, on the other hand, is found to increase more strongly near the surface and less so (or even to decrease) aloft. The overall number concentration of accumulation and coarse mode aerosol particles decreases (except right at the surface in summer and autumn), however, due to a lower emission rate. This results in a general decrease in the number concentration of immersed aerosol particles available for ice nucleation (Figure 7), despite an increase in the fraction of particles activated into cloud droplets.

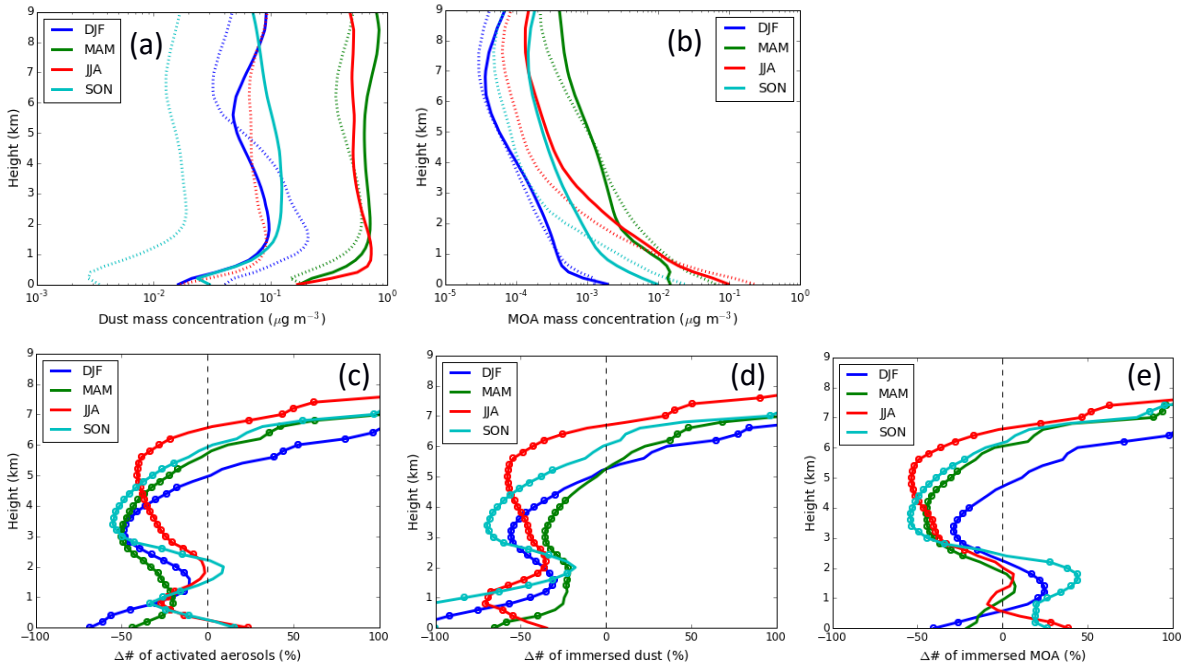

Figure 7: Arctic-wide (north of 75° N) seasonal mean vertical profiles of the PD (solid lines) and future (dash lines) mass concentration of (a) dust aerosols and (b) MOA. Also shown are the relative changes [(future-PD)/mean] in (c) the number concentration of aerosol particles activated into cloud droplets and (d) the number concentration of dust aerosols and (e) MOA immersed in droplets. Circles indicate statistical significance at the 95 % level.

2.2 Changes in the environment

Climate change leads to an amplified temperature increase in the Arctic (Serreze and Francis, 2006). In our model, this translates to seasonal mean warming of 2 to 10 °C at the surface and 2 to 3 °C above 1.5 km height in the Arctic region (Figure 8a). Specific humidity increases with a similar but slightly different trend at different altitudes. This leads to a general increase in seasonal mean relative humidity (RH; Figure 8b) of less than 4 % below 2 km height (except autumn when there is a 5 % decrease in RH at the surface and up to 6 % increase peaking at around 1 km height). In the higher altitudes, however, there is a general decrease in RH of up to 3 %.

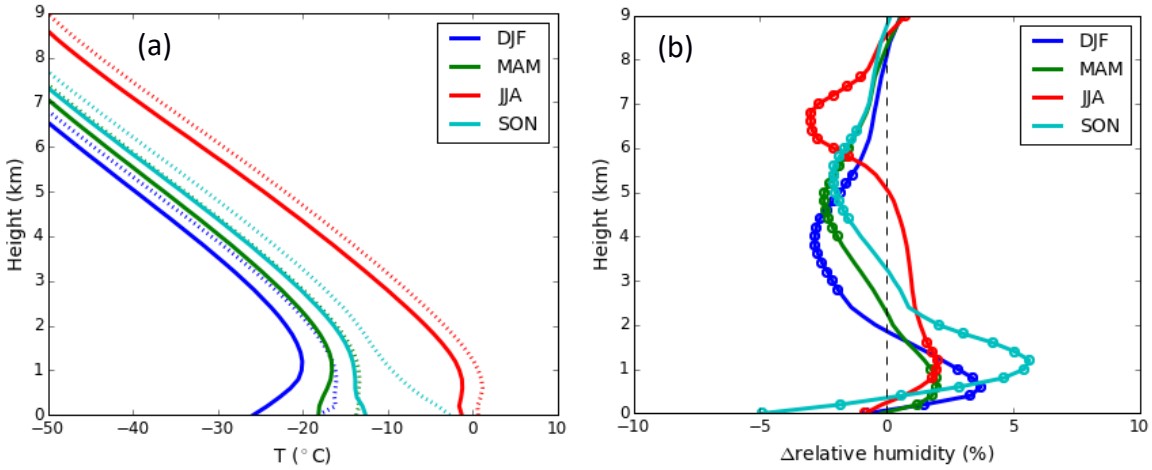

Figure 8: Arctic-wide (north of 75° N) 10-year seasonal mean vertical profiles of (a) temperature in the PD (solid lines) and in the future (dash lines), and (b) the absolute change (future-PD) in relative humidity. Circles in (b) indicates statistically significant changes at the 95 % level.

2.3 Changes in heterogeneous ice nucleation in the future

2.3.1 Freezing rate during occurrence

Heterogeneous ice nucleation in the Arctic can change in the future due to changes in both INP concentrations and the environmental condition that these aerosols are exposed to. As discussed previously, the concentration of dust aerosols decreases strongly in the Northern Hemisphere in the future in our model while MOA concentrations show a non-statistically significant increase near the surface and decrease aloft. The changes in aerosol concentrations, therefore, are likely to induce a decrease in heterogeneous ice nucleation rate in the Arctic except near the surface where contributions from MOA may lead to an increase in freezing rate.

Changes in the environment, on the other hand, are dominated by increases in temperature. Since the ice activity of both MOA and dust decreases sharply with increasing temperature, the upward shifting of isotherms is expected to contribute to a decrease in heterogeneous ice nucleation rate at each altitude in the future.

When considered together, the significant decrease in dust concentration and increase in temperature is expected to dominate, and this is indeed the case as shown in Figure 9a,b,

where the freezing rate during occurrence of MOA and dust are both shown to decrease by around 50 to 200 % in the future (except at the surface in summer for MOA).

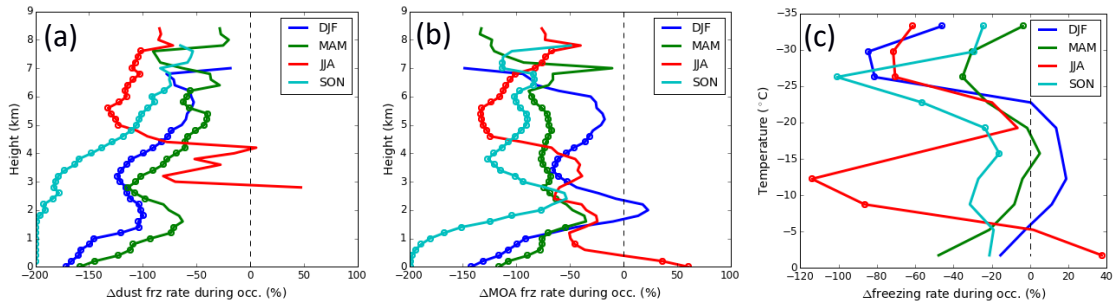

Figure 9: Arctic-wide (north of 75° N) seasonal mean vertical profiles of relative changes [(future-PD)/mean] in droplet freezing rate during occurrence due to (a) dust aerosols and (b) MOA plotted against height and (c) of both species combined plotted against temperature bins. Circles indicate statistical significance at the 95 % level.

To rule out influences due to shifting of the isotherms, the freezing rate is binned by temperature in each time step and averaged over the respective periods. The relative difference between the future and PD is then taken for each temperature bin (Figure 9c). Here a decrease in freezing rate during occurrence of around 20 to 100 % can still be noted, especially at temperatures colder than -20 °C which mostly occur at altitudes above 2 km where INP concentrations decrease considerably. The decreasing trend is extended to warmer temperatures in summer when the isotherm at 2 km is closer to -5 °C on average. An exception is during summer for the warmest temperature bin, where statistically significant increase in the freezing rate during occurrence can also be observed, resulting from the significant increase in MOA concentration near the surface.

All other seasons do not exhibit a significant change in freezing rate at the warmer temperatures. This is because MOA dominates over dust as the more ice-active INP at these temperatures, and the change in the number concentration of immersed MOA available for ice nucleation is more variable and less statistically significant at levels below 2 km where these temperatures tend to occur. In particular, during winter, the average temperature is generally below -15 °C at all levels and higher temperatures are rare.

Notably, significant increases in the number of immersed MOA can be observed during autumn at all levels below 2.5 km (Figure 7e) but no notable increases in the freezing rate during occurrence can be seen in any of the temperature bins (Figure 9c). Closer examination of the temperature changes reveals that during this season, temperatures warm on average by 3 to 10 °C in the Arctic, which would result in shifts across temperature bins (each with width of 3.5 °C). As the MOA concentration is highest close to the surface and sharply decreases aloft (Figure 7b), shifts in isotherms can result in statistically insignificant changes in the freezing rate during occurrence at each temperature despite relative increases in MOA concentration at all levels.

2.3.2 Frequency of freezing occurrence

In terms of the frequency at which heterogeneous ice nucleation occurs in the Arctic, PD conditions lead to the most frequent occurrence near the surface below 1 km altitude in our

model. MOA causes nucleation of ice crystals during up to 17 % of the time steps in winter and 45 % in summer. Dust, on the other hand, nucleates ice only during up to around 13 % of the time in all seasons except summer, when the peak freezing occurrence takes place at around 5 km altitude but occurs only around 5 % of the time, due to the limited temperature range at which nucleation of ice crystals on dust INP is relevant.

In the future, a general increase in ice nucleation occurrence is found at higher levels compared to the PD due to upward shifting of the isotherms, while closer to the surface the frequency decreases during warmer seasons as the temperature more frequently becomes too warm for the relevant nucleation process (Figure 10a,b). Again, examining the changes for a given temperature bin (Figure 10c,d,e) reveals more frequent freezing occurrence by up to 100 % of the time at warmer temperatures (> -15 °C in spring and autumn and > -23 °C in winter; Figure 10c) and less frequent occurrence at colder temperatures. In summer, the decrease in freezing occurrence takes place mainly at the warmer temperatures (-13 °C to -5 °C) and only a slight increase can be noted for the warmest temperature bin. These trends mostly reflect the seasonal changes in the frequency of occurrence of the respective temperatures in each bin (Figure 10d).

Ruling out the changes due to the increasing temperature, the frequency of freezing during temperature occurrence is shown in Figure 10e. Here it can be observed that the strong increase in occurrence frequency at warmer temperatures is largely diminished. Instead, there is a notable decrease in nucleation frequency at the colder temperatures in autumn, increase in the medium temperature range in winter, and decrease at the warmer temperatures in summer. As immersion freezing requires that the INP particles be immersed in cloud droplets for freezing to occur, the frequency of occurrence can also be controlled by the availability of such liquid droplets. Indeed, a similar trend in the change in the supercooled liquid fraction (which indicates the change in amount of droplets available for freezing) can be observed (Figure 10f) as described above for the change in freezing frequency during each temperature occurrence (Figure 10e).

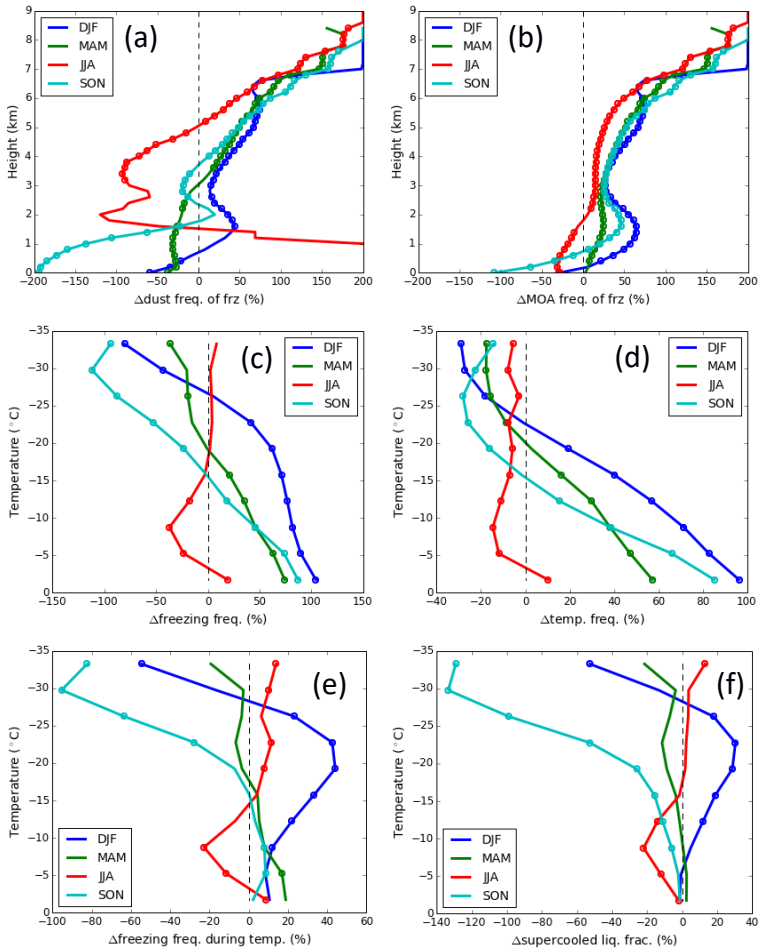

Figure 10: Arctic-wide (north of 75° N) seasonal mean vertical profiles of relative changes [(future-PD)/mean] in freezing occurrence frequency due to (a) dust aerosols and (b) MOA plotted against height and (c) of both species combined plotted against temperature bins. The relative change in frequency of occurrence of each temperature bin is shown in (d) and that in freezing frequency during temperature occurrence in (e). Additionally, the relative change in the supercooled liquid fraction is shown in (f). Circles indicate statistical significance at the 95 % level.

2.3.3 Overall freezing rate

Combining the changes in both the freezing rate during occurrence and frequency of occurrence, future changes in the overall contribution of heterogeneous ice nucleation in the Arctic are shown in Figure 11. Contributions by MOA and dust particles as INPs decrease by 50 to 200 % throughout all levels (except in summer near the surface, with an increase by nearly 50 %). Binned by temperature, the overall freezing rate decreases by 20 to 150 %, with the exception of winter when the increased occurrence of the warmer temperatures and increased presence of supercooled liquid droplets at the medium mixed-phase temperature range result in more ice nucleation at these temperatures. Additionally, freezing contributions from the warmest temperature bins also increase in summer and autumn, attributable to increases in the freezing rate during occurrence (summer) and frequency of occurrence (autumn). By comparing Figure 11b to Figure 9c, the contribution of changes in freezing occurrence frequency (mostly due to increasing temperatures and changes in the available liquid droplets) to the overall freezing rate can be approximated. The most notable differences are in winter for temperatures above -20 °C and in autumn for the highest temperature bins,

where increases in occurrence frequency in the future contributes to an increase in freezing of around 70 %. For the coldest mixed-phase temperature bins, less frequent freezing occurrence contribute to a 20 to 120 % decrease in heterogeneous ice nucleation for all seasons except summer (when the temperature change is minimum between PD and the future, as shown in Fig. 8a).

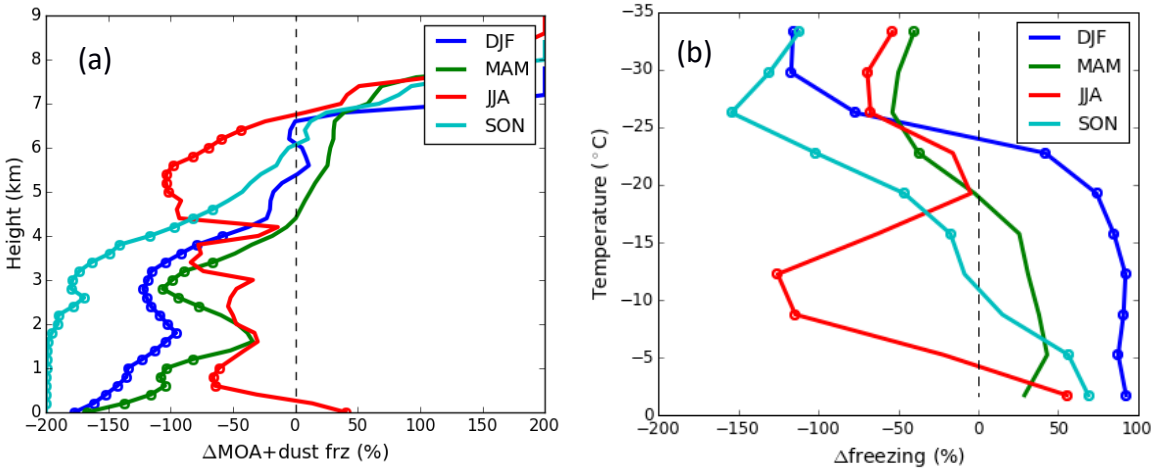

Figure 11: Arctic-wide (north of 75° N) seasonal mean vertical profiles of relative changes [(future-PD)/mean] in overall droplet freezing rate plotted against (a) height and (b) temperature bins. Circles indicate statistical significance at the 95 % level.

2.4 Conclusions

Summarising from the above-discussed results, a 50 to 200 % decrease in mean freezing rate is observed in the Arctic in the future (2050), except near the surface in summer where an average increase of nearly 50 % can be noted. When inspected by temperature bins, this can be attributed to a decrease in freezing contribution from colder mixed-phase temperatures due to both warming in the Arctic and decreases in INP concentrations. An increase in freezing contribution from warmer mixed-phase temperatures, on the other hand, can be mainly traced back to warming temperatures in winter and autumn and to aerosol changes in summer. Lastly, shifting of the isotherms in an environment where the INP concentration is strongly decreasing with altitude and thus confined to near the surface as for MOA results in negligible changes in freezing rate despite an overall increase in concentration at all levels in autumn.

3. Impact of ship emissions in a future ice-free Arctic ocean

We analysed how aerosol particles, clouds, and their impacts on radiation might change in the future when part of the Arctic sea ice melted (Gilgen et al., ACPD, 2017, in review). Simulations with the global aerosol-climate model ECHAM6-HAM2 were conducted for the years 2004 and 2050 and focus was placed on the periods late summer (July/August) and early autumn (September/October). Next to changes in natural aerosol emissions, the impact of enhanced Arctic shipping activity in the future was considered. The future ship emissions are based on the study by Peters et al. (2011) and consider changes in shipping related to transport and oil/gas extraction. In the simulations, the sea ice area decreases from $6.1*10^6$ km² to $3.4*10^6$ km² and from $5.7*10^6$ km² to $2.3*10^6$ km² in late summer and early autumn, respectively;

present-day sea ice area is derived from observations, whereas the future sea ice area is based on future simulations from the Earth-System-Model MPI-ESM (RCP8.5).

Sea ice acts as a barrier between the ocean and the atmosphere, therefore the decrease in the sea ice area leads to higher emissions of natural aerosol particles (sea salt) and precursors gases (DMS) in the future. As an example, the vertically integrated mass of sea salt between 75° and 90°N increases by 90% in early autumn.
Both changes in aerosol particles and meteorology lead to an increase in cloud droplet number concentrations (+29% in-cloud/+35% all-sky between 75° and 90°N in early autumn). Furthermore, not only the number concentration, but also the size of the cloud droplets increases, which is due to the higher specific humidity in the future.
The cooling effect of both aerosol particles and clouds is larger in the future, especially in late summer when more sunlight is available in the Arctic. However, this is not predominantly caused by changes in the aerosol particles and clouds themselves, but by changes in the surface albedo. The radiative effects of aerosols and clouds strongly depend on the surface albedo; as an example, aerosol particles can have a cooling effect if the surface is dark, but a warming effect if the surface is bright. The reduction in sea ice, which is highly reflective, thus increases the cooling component of aerosols and clouds. Averaged between 75° and 90°N, the radiative forcing of aerosols decreases from 0.53 Wm^{-2} to 0.36 Wm^{-2} and the cloud radiative effect from -36 Wm^{-2} to -46 Wm^{-2} in late summer.

To detect significant changes in aerosol particles, the ship emissions by Peters et al. (2011) had to be increased by a factor of 10 in terms of mass. The reason is that aerosol particles from other sources, which are transported to the Arctic Ocean, dominate the aerosol concentrations. This scaling can be seen as an upper estimate based on recent findings about the black carbon (BC) ship emission factors (McKuin and Campell, 2016) and on the comparison with other studies (e.g. Corbett et al., 2010).
Despite the tenfold ship emissions, changes in the aerosol radiative forcing were small and insignificant. The radiative forcing of BC deposited on snow shows locally significant increases in early autumn (see Figure 12f), but both absolute values ($19*10^{-2}$ Wm^{-2}; averaged between 75° and 90°N) and absolute changes ($0.64*10^{-2}$ Wm^{-2}; not statistically significant over 75° to 90°N) are small. However, we find that the tenfold ship emissions clearly enhance the cooling effect of clouds in late summer (see Figure 12d). The increase in aerosol particles leads to more cloud droplets (see Figure 12b), which increases the total surface area of the clouds. Furthermore, the collision-coalescence process is less efficient, which increases the liquid water content of the clouds. Averaged between 75° and 90°N, the net cloud radiative effect decreases from -48 Wm^{-2} to -52 Wm^{-2}. Since the changes in clouds have a much larger impact than the changes in deposited BC, the simulations indicate that future Arctic shipping could lead to a small cooling that offsets part of the expected Arctic warming. However, this cooling is likely overestimated in these simulations since the ship emissions were scaled up by a factor of ten.

Only ship-induced changes in aerosols were accounted for in this study, but not changes in e.g. ozone. Furthermore, sea salt emission parameterisations, freezing mechanisms in clouds, and aerosol-cloud interactions (to name a few) are still very uncertain in global climate models. More investigations are therefore needed to refute or confirm the findings of this study.

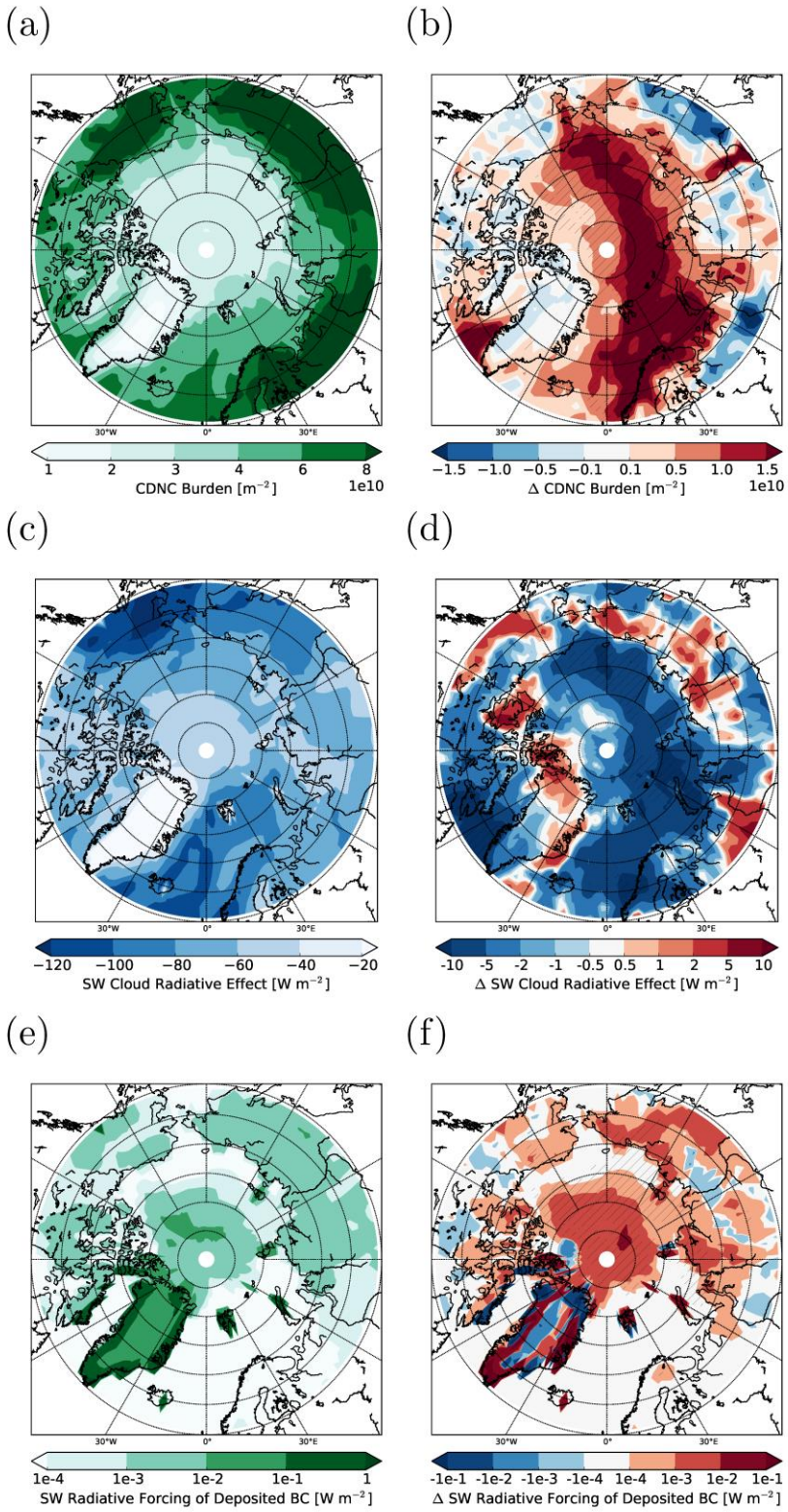

Figure 12: The impact of enhanced Arctic shipping on b) the vertically integrated cloud droplet number concentration, d) the shortwave cloud radiative effect, and f) the radiative forcing of BC deposited on snow. In (a), (c), and (e), the reference without additional ship emissions is shown. Hatched areas are significant at the 95% confidence level. (a) to (d) are shown for late summer, (e) and (f) for early autumn. Note that the scale in e) and f) is logarithmic.

4. Future impacts of wildfire and BVOC emissions to CCN

Improved emission fields for past and future BVOC and fire emissions under changing climate, landuse, [CO2] and vegetation have been produced within BACCHUS task 2.1 & 4.1 based on the LPJ-GUESS model and where used as input to BACCHUS task 4.5. BVOC emissions included monthly emissions for both Isoprene and monoterpene over the period 1901-2100. LPJ-GUESS was forced with MPI-ESM climate only as very similar results were obtained based on other climate forcing (see supplementary Hantson et al., 2017). These BVOC emissions estimates lay below estimated from other modeling groups (e.g. MEGAN). More detailed information regarding the BVOC emissions can be found in Hantson et al. (2017).

Fire emissions were estimated using the SIMFIRE model included into LPJ-GUESS (Knorr et al., 2016). For the period 2010-2100 we use the mean fire emissions from LPJ-GUESS-SIMFIRE when forced with climate data from 8 ESM's based on the RCP emission pathways and SSP2 socio-economical pathway. Fire emissions were scaled to GFED4s emissions to avoid as much as possible any impact by structure model biases. For data of the last century until 2010 we used the dataset for CMIP6 covering 1750-2015 (see van Marle et al., 2017).

The LPJ-GUESS simulated BVOC and wildfire emissions were included in ECHAM5.5-HAM2 simulations. The experiments focused on the period 2010–2100, and consisted of 10 timeslice simulations. The BVOC and wildfire emissions were averaged over 10 years around the simulated timeslice (±5 years), and one year nudged atmosphere-only simulation was analysed. Nudging was for 2010 meteorology for all simulations. Three sets of simulations were performed: either wildfire or BVOC emission perturbation was included, or both sources were allowed to change during 2010–2100.

During the 2010–2100 time period, the globally decreasing BVOCs lead to distinct changes in aerosol concentrations. First, the decrease in BVOCs induces a decrease in organic aerosol (OA) formation. From present-day (2010) values, the annual-average global monoterpene and isoprene emissions decrease by 24%, resulting in OA surface concentration decrease of 8.4% until year 2100. However, feedbacks in aerosol dynamics complicates the picture of number concentration response. CCN at 0.2% supersaturation, corresponding to larger particles (accumulation mode in M7), show a decreasing trend consistent with OA concentrations. However, decreasing OA concentrations are also reflected in lowered condensation sink, allowing for higher simulated sulfuric acid concentrations and consequently nucleation rates. This leads eventually to higher CN and even CCN(1.0%) concentrations in e.g. North America, Amazon, and South Africa.

Overall, Northern Hemisphere summer (JJA) global-average CCN(0.2%) concentrations are decreasing rather steadily after year 2060, and in 2100 CCN(0.2%) concentrations are 0.4% lower than in present-day (Figure 13). The opposite is true for CCN(1.0%), which until 2100 increases by 0.6% compared to 2010 values. In the case of changing wildfire emissions, the annual (or JJA) variability in CCN is less than 0.2%, and the difference between response of CCN at different supersaturations is rather similar. The trend in overall CCN when combining changes in wildfires and BVOCs (black lines in Figure 13) seem to be dominated by the BVOC changes.

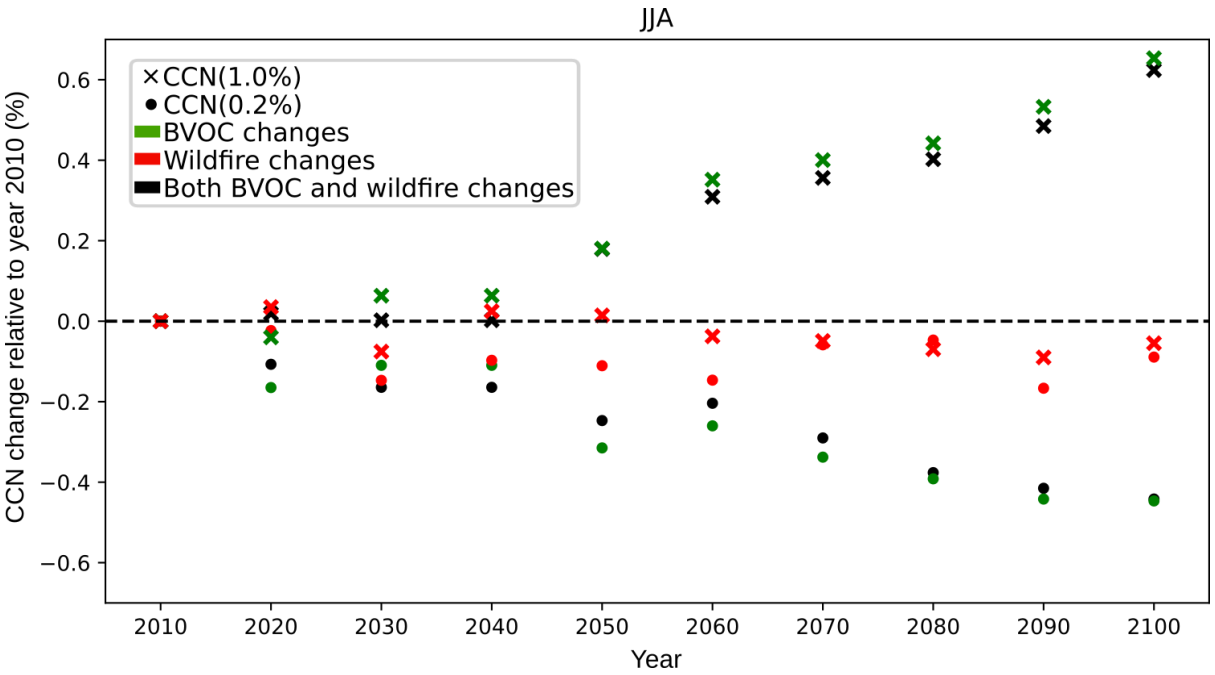

Figure 13: Changes in June-July-August CCN (at 0.2% and 1.0% supersaturation) relative to year 2010, shown for simulations including 1) only changes in BVOC emission (green), 2) only changes in wildfire emissions (red) and 3) simulations combining both changes in BVOC and wildfire emissions.

Figure 14 shows the global distribution of June-July-August CCN(1.0%) concentration change due to BVOC emission change between years 2010 and 2100. As discussed earlier, decreases in BVOC emissions lead to an increase in CCN(1.0%) in ECHAM-HAM simulations. As an example, Figure 14 reveals the underlying changes in aerosol dynamical parameters in North America, where CCN(1.0%) signal seems strong. At first step, BVOC-decrease results in decreasing organic growth rates as well as condensation sink (less organic aerosols). Second, the decrease in condensation sink both increases available gas-phase sulfuric acid resulting in increased nucleation rates. Even with reduced growth rates due to less organic vapours, the decreasing condensation sink seems to allow for higher survival rates for nucleated particles to reach 3 nm size (higher J3). Lastly, in our simulations the increased formation rate of 3 nm particles seems to be efficiently growing to Aitken mode (CCN(1.0%)) in e.g. North America.

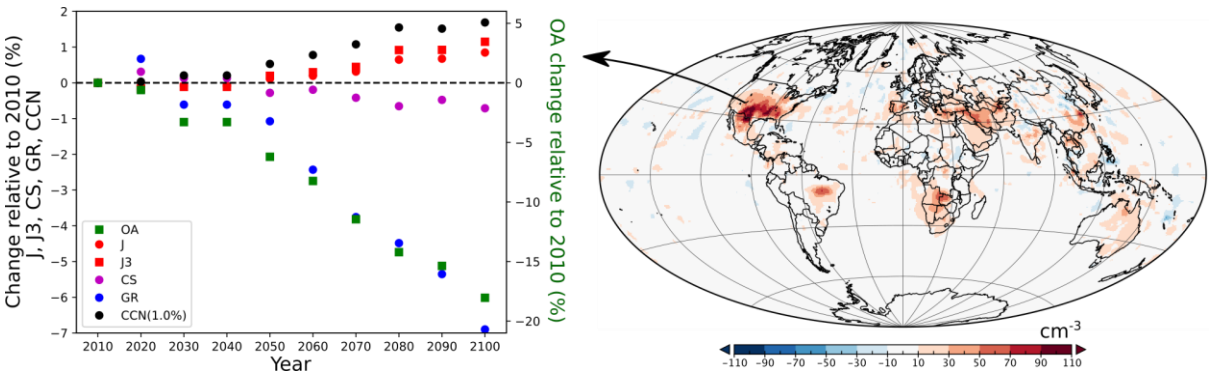

Figure 14: Trends in nucleation rate (J), formation rate at 3 nm (J3), condensation sink (CS), growth rate (GR), CCN(1.0%) and organic aerosol burden (OA) (left panel) and map of June-July-August CCN(1.0%) change between years 2010 and 2100 (right panel).

It should be kept in mind that the aerosol dynamical response and competition between nucleation and condensation in ECHAM-HAM simulations might be biased: earlier work has

shown that ECHAM-HAM can exhibit too high sensitivity of nucleation rates to background aerosol. Furthermore, we focused in this work to the CCN response to BVOC and wildfire sources. In the future, this should be coupled to the underlying changes in anthropogenic aerosol and precursor fluxes.

Changes with respect to DoW

The deliverable D4.5 was designed to apply the latest versions of three BACCHUS Earth System Models, which are not only developed in BACCHUS but also for large international activities such as CMIP6. Due to unforeseen delays in CMIP6 model development, the BACCHUS groups met difficulties in finding coupled CMIP6 Earth System Models for future scenario simulations. Hence, WP4 decided to focus D4.5 efforts towards one model (MPI-ESM) to answer the scientific topics in detail: preparation of ESM towards future scenario simulations, future ice nucleation in the Arctic, as well as impact of future ship, wildfire and BVOC emissions.

References:

Bathiany, S., Claussen, M., and Brovkin, V.: CO2-Induced Sahel Greening in Three CMIP5 Earth System Models, Journal of Climate, 27, 7163–7184, doi:10.1175/JCLI-D-13-00528.1, 2014.

Cheng, T., Peng, Y., Feichter, J., and Tegen, I.: An improvement on the dust emission scheme in the global aerosol-climate model ECHAM5-HAM, Atmos. Chem. Phys., 8, 1105–1117, doi:10.5194/acp-8-1105-2008, 2008.

Collins, M., R. Knutti, J. Arblaster, J.-L. Dufresne, T. Fichefet, P. Friedlingstein, X. Gao, W.J. Gutowski, T. Johns, G. Krinner, M. Shongwe, C. Tebaldi, A.J. Weaver and M. Wehner, 2013: Long-term Climate Change: Projections, Commitments and Irreversibility. In: Climate Change 2013: The Physical Science Basis. Contribution of Working Group I to the Fifth Assessment Report of the Intergovernmental Panel on Climate Change [Stocker, T.F., D. Qin, G.-K. Plattner, M. Tignor, S.K. Allen, J. Boschung, A. Nauels, Y. Xia, V. Bex and P.M. Midgley (eds.)]. Cambridge University Press, Cambridge, United Kingdom and New York, NY, USA.

Corbett, J. J., Lack, D. A., Winebrake, J. J., Harder, S., Silberman, J. A., and Gold, M.: Arctic shipping emissions inventories and future scenarios, Atmos. Chem. Phys., 10, 9689–9704, doi:10.5194/acp-10-9689-2010, 2010.

Flato, G., J. Marotzke, B. Abiodun, P. Braconnot, S.C. Chou, W. Collins, P. Cox, F. Driouech, S. Emori, V. Eyring, C. Forest, P. Gleckler, E. Guilyardi, C. Jakob, V. Kattsov, C. Reason and M. Rummukainen, 2013: Evaluation of Climate Models. In: Climate Change 2013: The Physical Science Basis. Contribution of Working Group I to the Fifth Assessment Report of the Intergovernmental Panel on Climate Change [Stocker, T.F., D. Qin, G.-K. Plattner, M. Tignor, S.K. Allen, J. Boschung, A. Nauels, Y. Xia, V. Bex and P.M. Midgley (eds.)]. Cambridge University Press, Cambridge, United Kingdom and New York, NY, USA.

Folini et al., 2018, in preparation

Gilgen, A., Huang, W. T. K., Ickes, L., Neubauer, D., and Lohmann, U.: How important are future marine and shipping aerosol emissions in warming Arctic summer and autumn?, Atmos. Chem. Phys. Discuss., https://doi.org/10.5194/acp-2017-1007, in review, 2017.

Hantson, S., Scheffer, M., Pueyo, S, Xu, C., Lasslop, G., van Nes, E., Holmgren, M. and Mendelsohn, J.: Rare, Intense, Big fires dominate the global tropics under drier conditions, Scientific Reports, volume 7, 14374, 2017.

Huang, W. T. K., Ickes, L., Tegen, I., Rinaldi, M., Ceburnis, D., and Lohmann, U.: Global relevance of marine organic aerosols as ice nucleating particles, Atmos. Chem. Phys. Discuss., doi: 10.5194/acp-2017-922, in review, 2017.

Jungclaus, J. H., Fischer, N., Haak, H., Lohmann, K., Marotzke, J., Matei, D., Mikolajewicz, U., Notz, D., and von Storch, J. S.: Characteristics of the ocean simulations in the Max Planck Institute Ocean Model (MPIOM) the ocean component of the MPI-Earth system model, J. Adv. Model. Earth Sy., 5, 422–446, https://doi.org/10.1002/jame.20023, 2013.

Kanji, Z. A., Ladino, L. A., Wex, H., Boose, Y., Burkert-Kohn, M., Cziczo, D. J., and Krämer, M.: Overview of Ice Nucleating Particles, Meteor. Mon., 58, 1.1–1.33, doi:10.1175/AMSMONOGRAPHS-D-16-0006.1, 2017.

Knorr, W., Dentener, F., Hantson, S., Jiang, L., Klimont, Z., and Arneth, A.: Air quality impacts of European wildfire emissions in a changing climate, Atmos. Chem. Phys., 16, 5685-5703, https://doi.org/10.5194/acp-16-5685-2016, 2016.

Massonnet, F., T. Fichefet, H. Goosse, C. M. Bitz, G. Philippon-Berthier, M. Holland, and P. Y. Barriat, 2012: Constraining projections of summer Arctic sea ice. Cryosphere, 6, 1383–1394.

McKuin, B. and Campbell, J. E.: Emissions and climate forcing from global and Arctic fishing vessels, J. Geophys. Res.-Atmos., 121, 1844–1858, doi:10.1002/2015JD023747, 2015JD023747, 2016.

Morrison, H., de Boer, G., Feingold, G., Harrington, J., Shupe, M. D., and Sulia, K.: Resilience of persistent Arctic mixed-phase clouds, Nature Geoscience, 5, 11–17, doi:10.1038/ngeo1332, 2012.

Peters, G. P., Nilssen, T. B., Lindholt, L., Eide, M. S., Glomsrød, S., Eide, L. I., and Fuglestvedt, J. S.: Future emissions from shipping and petroleum activities in the Arctic, Atmos. Chem. Phys., 11, 5305–5320, doi:10.5194/acp-11-5305-2011, 2011.

Phillips, A. S., C. Deser, and J. Fasullo, 2014: A New Tool for Evaluating Modes of Variability in Climate Models. EOS, 95, 453-455, doi: 10.1002/2014EO490002.

Phillips, A. S., C. Deser, and J. Fasullo, 2014: A New Tool for Evaluating Modes of Variability in Climate Models. EOS, 95, 453-455, doi: 10.1002/2014EO490002.

Pruppacher, H. and Klett, J.: Microphysics of Clouds and Precipitation, Springer, 2 edn., 1997.

Rotstayn LD, Collier MA, Shindell DT, Boucher O. Why does aerosol forcing control historical global-mean surface temperature change in CMIP5 models? J Clim. 2015;28(17):6608–25. https://doi.org/10.1175/JCLI-D-14-00712.1

Serreze, M. C. and Francis, J. A.: The Arctic Amplification Debate, Climatic Change, 76, 241–264, doi:10.1007/s10584-005-9017-y, 2006.

Shupe, M. D.: Clouds at Arctic Atmospheric Observatories. Part II: Thermodynamic Phase Characteristics, Journal of Applied Meteorology and Climatology, 50, 645–661, doi:10.1175/2010JAMC2468.1, 2011.

Stevens, B., Giorgetta, M., Esch, M., Mauritsen, T., Crueger, T., Rast, S., Salzmann, M., Schmidt, H., Bader, J., Block, K., Brokopf, R., Fast, I., Kinne, S., Kornblueh, L., Lohmann, U., Pincus, R., Reichler, T., and Roeckner, E.: Atmospheric component of the MPI-M Earth System Model: ECHAM6, J. Adv. Model. Earth Syst., 5, 146–172, doi:10.1002/jame.20015, 2013.

Tegen, I., Harrison, S. P., Kohfeld, K., Prentice, I. C., Coe, M., and Heimann, M.: Impact of vegetation and preferential source areas on global dust aerosol: Results from a model study, J. Geophys. Res., 107, 4576, doi:10.1029/2001JD000963, 2002.

Tegen, I., Lohmann, U., Neubauer, D., Siegenthaler-Le Drian, C., Ferrachat, S., Bey, I., Stanelle, T., Stier, P., Schutgens, N., Watson-Parris, D., Schmidt, H., Rast, S., Schultz, M. G., Schroeder,

S., Kokkola, H., Barthel, S., and Heinold, B.: The aerosol-climate model ECHAM6.3-HAM2.3: Aerosol evaluation, Geosci. Model Dev. Discuss., in preparation, 2018.

van Marle, M. J. E., Kloster, S., Magi, B. I., Marlon, J. R., Daniau, A.-L., Field, R. D., Arneth, A., Forrest, M., Hantson, S., Kehrwald, N. M., Knorr, W., Lasslop, G., Li, F., Mangeon, S., Yue, C., Kaiser, J. W., and van der Werf, G. R.: Historic global biomass burning emissions for CMIP6 (BB4CMIP) based on merging satellite observations with proxies and fire models (1750–2015), Geosci. Model Dev., 10, 3329-3357, https://doi.org/10.5194/gmd-10-3329-2017, 2017.